Microwave Photonics Filtering Technique for Interrogating a Very-Weak Fiber Bragg Grating Cascade Sensor
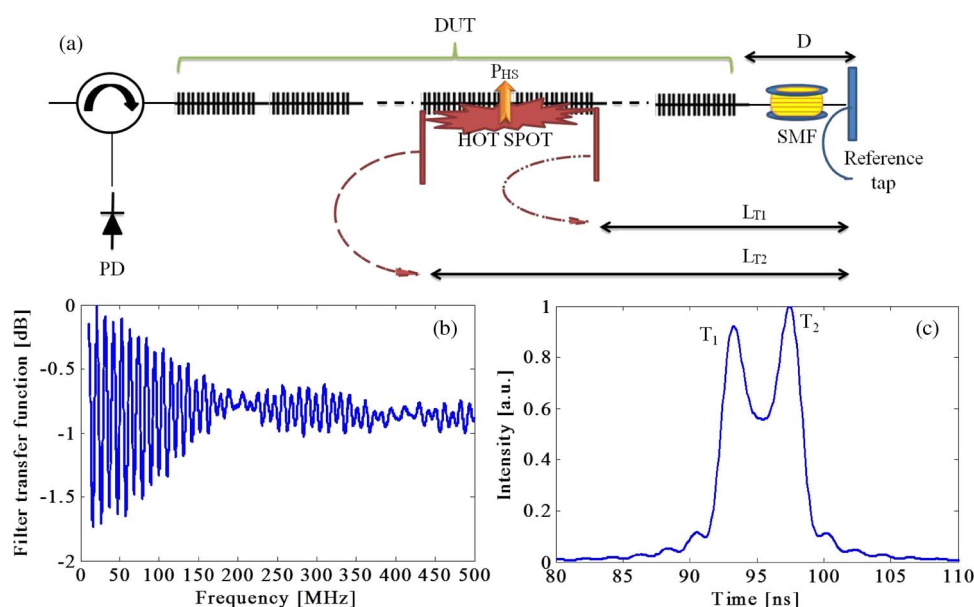
A. L. Ricchiuti
J. Hervás
D. Barrera
S. Sales
J. Capmany

Microwave Photonics Filtering Technique for Interrogating a Very-Weak Fiber Bragg Grating Cascade Sensor

A. L. Ricchiuti, J. Hervás, D. Barrera, S. Sales, and J. Capmany

ITEAM Research Institute, Universidad Politécnica de Valencia, 46022, Valencia, Spain

Abstract: A system to interrogate photonic sensors based on a very weak fiber Bragg grating cascade fiber is presented and experimentally validated and dedicated to detecting the presence and location of a spot event. The distributed sensor proposed consists of a 5-m-long fiber, containing 500 9-mm-long Bragg gratings with a grating separation of 10.21 mm. The principle of operation is based on a technique used to analyze microwave photonics filters. The detection of spot events along the sensor is demonstrated with remarkable accuracy under 1 mm, using a photodetector and a modulator with a bandwidth of only 500 MHz. The simple proposed scheme is intrinsically robust against environmental changes and is easy to reconfigure.

Index Terms: Discrete-time sensor, fiber Bragg gratings (FBGs), fiber optic sensors, microwave photonics filters, weak FBGs.

1. Introduction

Fiber Bragg gratings (FBGs) play a key role as components in all-fiber based devices due to their advantageous characteristics such as simplicity, low insertion loss, low cost, polarization independence, and seamless integration in fiber optic systems. Furthermore, since FBGs are made of dielectric material, they are non conducting, immune to electromagnetic interference (EMI), chemically inert and spark free [1]. For these reasons FBGs have been extensively implemented in different kinds of application scenarios such as sensors [2], filters [3], switches [4], and for multiplying pulse repetition rates [5], amongst others.

As far as the sensing area is concerned, different methods and techniques have been proposed and implemented in order to interrogate the Bragg-frequency distribution along an FBG with the aim of implementing distributed temperature/strain sensors. Some of these salient techniques include optical low-coherence reflectometry (OLCR) [6], optical frequency domain reflectometry (OFDR) [7], synthesis of optical coherence function (SOCF) [8], and time-frequency analysis [9]. Recently, several methods have been proposed with the aim of implementing temperature/crack sensors; long FBGs have been used for detecting hot spots [10], and faint long gratings have been used as temperature sensors [11]. Photonics-assisted techniques
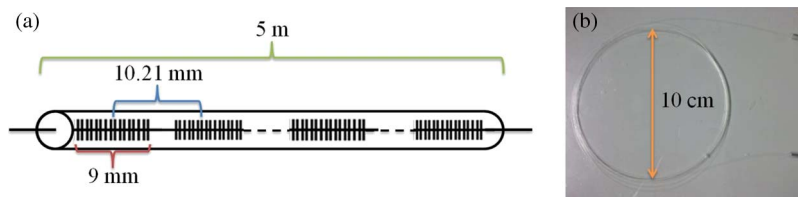
Fig. 1. (a) Schematic representation of the 5 m-long cascade sensor containing 500 weak FBGs. The nominal length of each FBG is 9 mm, and the separation between consecutive FBGs is 10.21 mm. (b) Fiber cascade sensor rolled up.

have raised increasing interest during the past decades not only from the research community but also from the commercial sector, leading to new possibilities in a variety of application fields, including microwave photonics (MWP) sensing [12]–[14].

In this work, a technique to interrogate very long FBG-based sensors and its potential applications to fiber sensing is proposed and demonstrated via experiments. This technique has several advantages derived from the fact that it relies on microwave rather than on optical interferences. Microwave interferometry is by far more stable and easier to control and, if suitably combined with photonics, provides a remarkable spatial accuracy. Furthermore, since the sensor is based on a discrete time filter configuration, the system spectral performance can be properly tailored/reconfigured. Thus, the methodology presented involves exploiting the best advantages brought by two symbiotic technologies: microwaves and photonics. Relying on microwave interferometry and working under incoherent operation, the configuration proposed is intrinsically robust against environmental changes, stable and with good repeatable performance [15], [16]. Finally, this technique is potentially low cost as it is based on low bandwidth radio-frequency (RF) and off-the-shelf photonic components rather than on ultra-short pulses, optical interferometry or OFDR techniques. The proposed system is specifically suited when a spot event must be precisely identified and located, such as hot-spots or cracks in structures. The fundamental concept for the proposed interrogation technique is inspired on the operation principle of a discrete time MWP filter [15], [16], in particular by the information gives on the delays between the different taps of the filter provided by measuring its RF transfer function provided by the S_{21} parameter. The proposed sensor is composed of an array of 500 equal very weak (reflectivity $= 0.001$) FBGs written in cascade in a 5 m-long optical fiber. The nominal length of each FBG is 9 mm and the separation between consecutive FBGs in the array is 10.21 mm, as shown in Fig. 1(a). The FBG cascade fiber was kindly provided by FBGS International [17], which fabricates optical fibers by using Draw Tower Gratings (DTGs) Technology. This technique combines the drawing of the optical fiber with the writing of the grating. During the production process a glass pre-form is heated and then the pulling and formation of the fiber is initiated. The FBG cascade sensor is continuously written using a pulsed excimer laser during the fiber drawing process. Pulse repetition rate is synchronized with the drawing speed in order to obtain an equal spacing between consecutive FBGs. This automated production process results in very high quality, accurately positioned FBGs which allows controlling the production parameters very accurately, thus assuring high repeatability and grating uniformity. Since FBG writing is previous to coating, the fiber could be rolled up in a compact coil of around 10 cm diameter, as shown in Fig. 1(b).

2. Principle of Operation

The setup used to interrogate the weak FBG cascade sensor is based on the principle of operation of a MWP filter and is depicted in Fig. 2(a). The output of a continuous wave (CW) light source is electro-optically modulated with a microwave (MW) signal. At the output of the electro-optical modulator (EOM) the modulated optical signal is split into N arms. Each arm contains a delay-line and an attenuator (or amplifier) in order to provide a delayed and weighted replica of
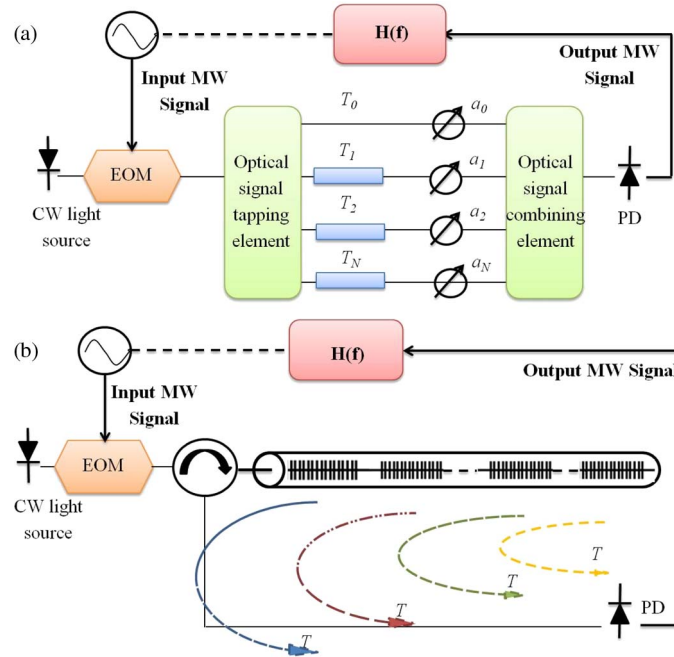
Fig. 2. (a) Schematic diagram representing an *N* tap microwave photonic filter. (b) Schematic diagram implemented for interrogating the weak FBGs cascade sensor using microwave photonic techniques.

the original signal. These time-delayed and weighted optical signals are combined together and finally photo-detected. In the detection process, the different taps can be mixed according to either a coherent or an incoherent basis. In case of incoherent mixing, the tap combination at the photo-detector (PD) is insensitive to environmental effects, stable and with a remarkably good repeatable performance. For these reasons, the experimental setup proposed has been implemented under incoherent operation. Working under incoherent regime limits the minimum delay between consecutive taps, which should be at least one order of magnitude greater than the source coherence time [10]. The MW signal is acquired, and the electrical response $H(\Omega)$ of such a structure is given by [16]

$$H(\Omega) = \sum_{k=0}^{N} a_k e^{-i\Omega T_k} \tag{1}$$

where Ω is the MW frequency, and a_k is the weight of the kth replica that is delayed by T_k.

The proposed sensor produces delayed replicas of the original signal at the place where each FBG is located, as shown in Fig. 2(b). As the spacing between consecutive FBGs is constant, $T_k = kT \ \forall k$, which means that (1) identifies a transfer function with a periodic spectral characteristic. The frequency period is known as *free spectral range* (FSR) and is inversely proportional to the spacing T between samples [16]. The MWP filter so created presents $N - 1$ minima between two consecutive maxima (i.e. one FSR). This way, the distance between minima in the electrical frequency response can be used to calculate the number of taps contributing to the filter frequency response. By evaluating the latter, the position and length of the hot spot along the sensor can be retrieved, as will be explained in the next section.

3. Experimental Measurements and Results

The setup implemented to interrogate the 5 m-long sensing device, named device under test (DUT), is illustrated in Fig. 3. The output of a broadband source (BBS) provided by a SuperLED
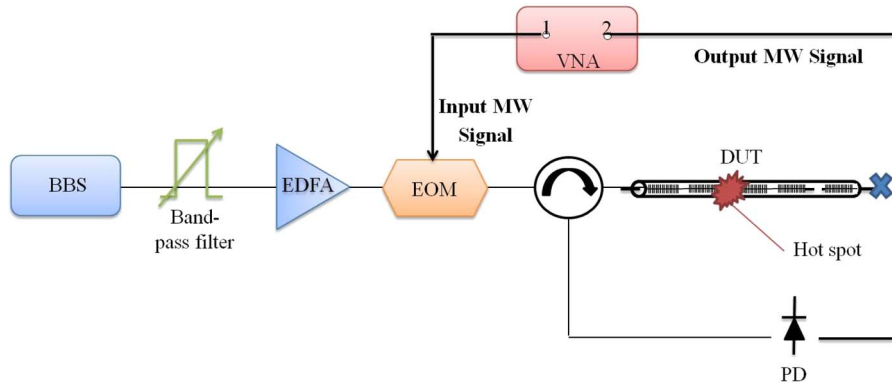
Fig. 3. Schematic diagram implemented for interrogating the weak FBG-based sensor.
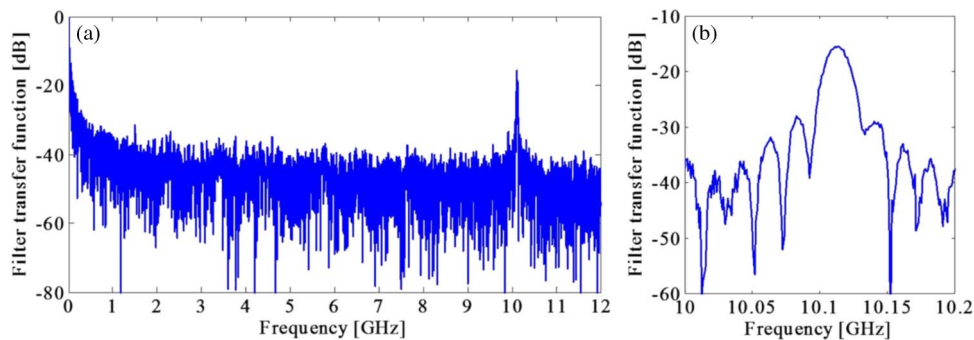

Fig. 4. (a) Transfer function of the MWP filter. (b) Detail of the filter transfer function showing the first main resonance.

is filtered by means of an optical tunable band-pass filter featuring a bandwidth of 1 nm centered at the nominal Bragg wavelength of the DUT. The main limitation of this technique arises from the fact that the conditions for incoherent regime operation have to be guaranteed. This implies that the minimum delay between two consecutive taps (i.e., two consecutive FBGs) must verify that $t_c \ll T$, where t_c is the optical source coherence time is given by [18]

$$t_c = \frac{1}{\Delta f} \tag{2}$$

where Δf is the spectral bandwidth of the optical filter. This way, as the band-pass filter bandwidth is 1 nm, the time coherence of the filtered optical source is 8 ps. The smallest time spacing which safely secures the incoherent regime operation would be an order of magnitude greater than this value. This implies that the distance between consecutive FBGs should be longer than 8.24 mm [10], [18]; as the separation between the FBGs in the array is 10.21 mm, the incoherent regime operation is guaranteed.

The output of the optical filter is amplified by means of an erbium doped fiber amplifier (EDFA), then electro-optically modulated with a MW signal generated by a vector network analyzer (VNA). At the output of the EOM, the modulated signal is sent into the DUT through an optical circulator. The signal reflected by the grating is finally photo-detected and the frequency response of the system is analyzed by monitoring the scattering parameter S_{21}, which relates the RF detected signal to the input modulating MW signal.

First, the MW tone provided by the VNA is swept from 10 MHz to 12 GHz in order to retrieve the electrical response of the system (described by the module of the scattering parameter S_{21}), which is illustrated in Fig. 4(a), while Fig. 4(b) shows the detail of the filter main resonance

around 10.11 GHz. The FBGs low reflectivity lets us assume that the incoming signal is back-reflected with almost the same weight from each of the 500 FBGs. The value of the first main resonance (i.e., the FSR span), is related to the distance d between two consecutive FBGs according to

$$d = \frac{c}{2n_0 FSR} \tag{3}$$

where c is the speed of light in vacuum and n_0 the effective refractive index of the DUT.

Similarly, taking advantage of this concept, the length of a spot event located along the sensing fiber can be calculated. In fact, as mentioned in the previous section, the filter presents $N - 1$ minima between two consecutive maxima. Hence, the distance between two minima (hereinafter FSR') can be used to calculate the number of taps contributing to the filter response. As the distance between consecutive FBGs d in the DUT is known, by evaluating the FSR' of the MWP filter response, the length L_{HS} of the hot spot can be calculated according to

$$L_{HS} = \frac{c}{2n_0 FSR'}. \tag{4}$$

To corroborate this assumption, an experiment is set up using a frequency span of 500 MHz. The reason for this choice is due to the fact that this frequency range allows a better discrimination of the FSR' on the one hand, and on the other, this moderate span enables the use of devices with modest bandwidth.

The tunable band-pass filter located after the BBS plays a fundamental role in both the data acquisition process and the hot spot temperature estimation. In fact, the progressive sweep of the central wavelength of the optical filter is synchronized with the data acquisition process. This way, the sensing response to the hot region can be maximized when the rise/fall slope is located as close as possible to the peak corresponding to the hot spot, as shown in Fig. 5(d). Fig. 5(a) shows the case in which the optical filter response is far from both the DUT original reflection and the hot spot reflection. In this condition, no signal will be back-reflected and the VNA only displays a noise trace. Fig. 5(c) represents the case in which both the DUT original reflection and the hot spot reflection are selected, while Fig. 5(b) and (d) illustrates the situation in which the band-pass of the filter is tuned in order to select the original reflection of the DUT and the hot spot reflection respectively. In these cases a frequency response of a MWP filter will be represented at the VNA monitor. Finally, by continuing to move the band-pass of the optical filter towards higher wavelengths (see Fig. 5(e)), again no signal will be reflected from the DUT. Hence, a noise trace will be displayed by the VNA. This way, by performing a wavelength scan of the input broad-band signal, the amplitude of the MWP filter response can be monitored and analyzed.

If no hot spots are located along the sensing device and the central wavelength of the optical filter is tuned in order to select the DUT original reflection, the electrical response of the system, obtained by sweeping the MW signal from 10 MHz to 500 MHz, can be retrieved as illustrated in Fig. 6(a) (blue curve), which is in agreement with the theoretical simulation (red curve). These initial results indicate that, as the MWP filter presents 500 taps (i.e., 499 minima between one FSR span), the frequency separation between two consecutive minima is $FSR' = 20.23$ MHz, confirming the theory described in the previous section. Now, it is worth noting that, in case of non-uniformity of the 500 FBGs will negatively affect the periodicity of the filter transfer function. But, the results in Fig. 6(a) show how the frequency response of the MWP filter representing the measured system response matches the frequency behavior of the simulated system response in the 500 MHz span. This fact leads us to consider the contribution of the possible grating non-uniformity negligible in the evaluation of the sensing performance.

Now, when a hot spot is placed along the 5 m-long sensing fiber, the heated surface suffers a period change which leads to a Bragg wavelength shift affecting the FBGs underlying the hot zone. If the optical filter is properly tuned in order to select the zone of the source spectrum
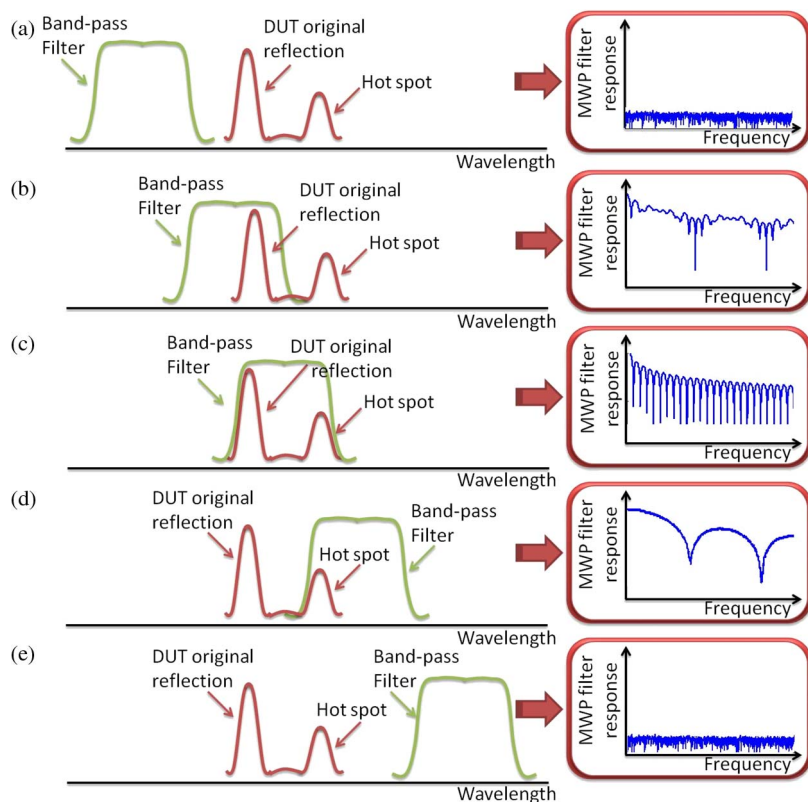
Fig. 5. Schematic of the optical band-bass filter central wavelength scan. (a) The filter response is far from both the DUT original reflection and the hot spot reflection. (b) The filter is tuned to select the DUT original response reflection. (c) The filter is tuned to select both the DUT original reflection and the hot spot reflection. (d) The filter is tuned to select the hot spot reflection. (e) The filter response is again far from both the DUT original reflection and the hot spot reflection.
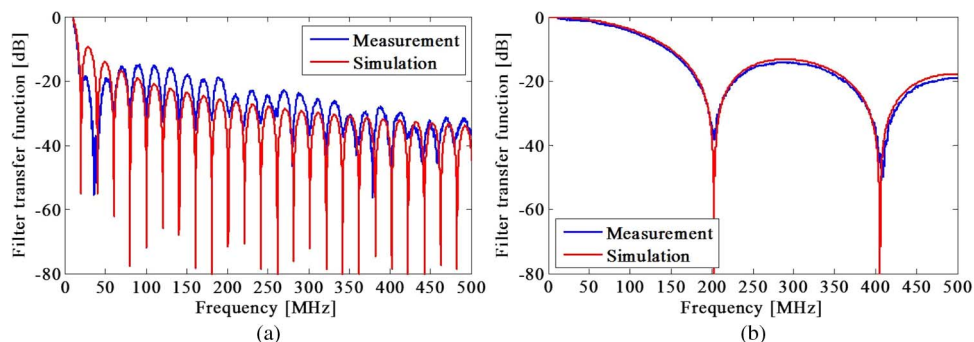

Fig. 6. (a) Frequency response of the MWP filter representing the measured (blue curve) and simulated (red curve) system response. (b) Frequency response of the MWP filter (measured and simulated) obtained by placing a hot spot along the DUT and by tuning the optical band-pass filter.

reflected by the heated FBGs (see Fig. 5(d)), the distance between minima in $H(\Omega)$ gives the length of the hot spot. This means that by evaluating the *FSR'* of the MWP filter depicted in Fig. 6(b) and using (4), the length of the hot zone is calculated to be 50.72 cm, with a spatial accuracy under 1 mm, dictated by the spatial resolution of the VNA.

Furthermore, in order to estimate the position of the spot event along the DUT, a piece of a single mode fiber (SMF) of length $D = 7$ m is appended at the end of the DUT, as illustrated in Fig. 7(a). The other end of the SMF is left open in the air to provide a reflection signal that will
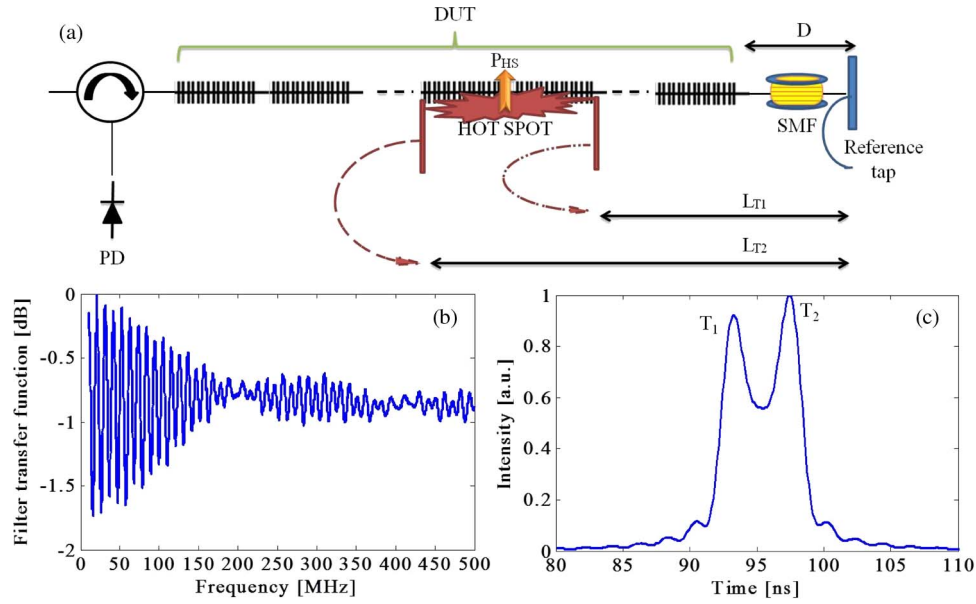
Fig. 7. (a) Schematic of the portion of the system used to retrieve the position of the hot spot. (b) Frequency response of the MWP filter obtained by placing a hot spot along the DUT and by using a reference tap. (c) Inverse Fourier transform of the MWP filter depicted in Fig. 7(b).

be used as a reference tap. The distance between one end of the hot spot and the end face of the SMF L_{T1}, and the distance between the other end of the hot spot and the end face of the SMF L_{T2} are related to the respective transit time between the end of the hot spot and the end face of the SMF T_1 and T_2 by

$$L_{T1} = \frac{cT_1}{2n_0} \tag{5}$$

$$L_{T2} = \frac{cT_2}{2n_0}. \tag{6}$$

Now, by opportunely tuning the optical band-pass filter in order to select only the hot spot corresponding reflection (see Fig. 5(d)) and by sweeping the MW signal from 10 MHz to 500 MHz, the transfer function of the MWP filter so obtained is detected, as shown in Fig. 7(b).

Since retrieving the delays directly from the transfer function is time consuming, the most efficient approach to calculate the distance between the middle point of the hot spot and the end of the DUT, is simply to take the inverse Fourier transform (IFT) of the measured S_{21} parameter, which is plotted in Fig. 7(c). In fact, the position of the middle point P_{HS} of the hot spot along the sensor can be calculated by

$$P_{HS} = \frac{(L_{T2} - D) + (L_{T1} - D)}{2} = \frac{L_{T2} + L_{T1}}{2} - D. \tag{7}$$

By using (5) and (6) in (7), one can find

$$P_{HS} = \frac{(T_2/2 + T_1/2)c}{2n_0} - D. \tag{8}$$

This way, the position of the hot spot middle point is measured from the DUT ending, resulting in $P_{HS} = 2.8440$ m.

As previously described, the temperature of the hot spot can be evaluated due to the progressive scan of the central wavelength of the tunable band-pass filter. Under this condition, based
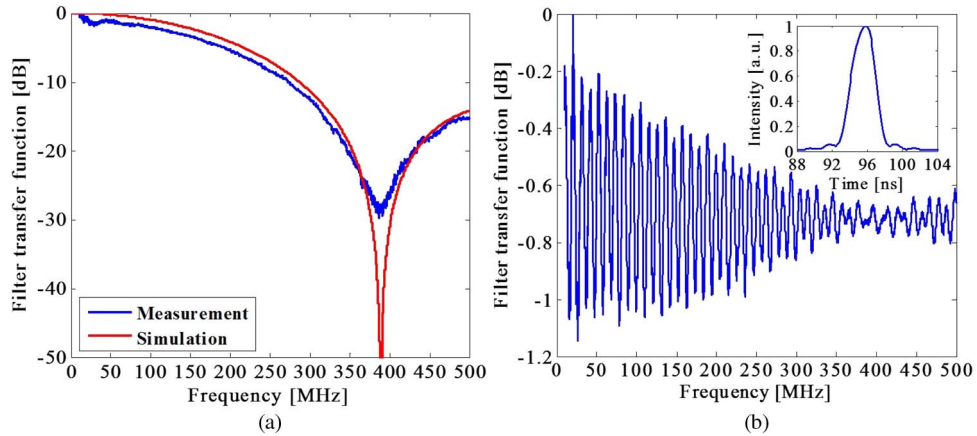
Fig. 8. (a) Frequency response of the MWP filter obtained by placing a 26.49 cm-long hot spot along the DUT. (b) Frequency response of the MWP filter obtained by placing a 26.49 cm-long hot spot along the DUT and by using the reference tap. Inset: IFT of the MWP filter.

on the fiber temperature coefficient, which is 16.855 pm/$^\circ$C, the temperature of the 50.72 cm-long hot spot is estimated to be around 70 $^\circ$C, with an accuracy of 1 $^\circ$C.

It is worth mentioning that since the filter formed by the taps provided by the hot spot has about two minima (see Fig. 6(b)), the proposed configuration can also be used to detect the presence and location of spot events shorter than 50 cm. In particular, the minimum detectable hot spot is directly related to the VNA frequency span Δf_{VNA}, according to

$$L_{HSmin} = \frac{1.5c}{2n_0 \Delta f_{VNA}}. \tag{9}$$

This means that by using a frequency span of 500 MHz the minimum measurable spot event is about 31 cm, if the methodology and the mathematical calculation so far detailed are used. Even so, shorter hot spots can still be detected in this frequency range. In order to validate this concept, a 26.49 cm-long hot spot is placed at a certain point of the DUT. The electrical response of the MWP filter, which is obtained by sweeping the MW signal from 10 MHz to 500 MHz, is depicted in Fig. 8(a). Once again, by evaluating the FSR' of the MWP filter response and by using (4), the length of the hot spot is calculated to be $L_{HS} = 26.49$ cm. Also, the position of the hot spot can be calculated by using the reference tap, similarly to the procedure previously described, and by employing the IFT of the resulting filter transfer function, which is illustrated in Fig. 8(b). As can be seen in the inset of Fig. 8(b), now the IFT presents only one peak, which is related to the position of the hot spot middle point. In this case, the location of the spot event can be calculated by retrieving the peak time position T' and by using

$$P_{HS} = \frac{T'c}{2n_0} - D. \tag{10}$$

This way, the location of the middle point of the hot spot along the sensor is estimated to be $P_{HS} = 2.8914$ m from the DUT ending.

Thus, the ultimate limit in the hot spot length and location results to be related to the VNA frequency span Δf_{VNA} according to

$$L_{HSmin} = \frac{c}{2n_0 \Delta f_{VNA}}. \tag{11}$$

4. Discussion and Future Directions

In this work, we have proposed and experimentally validated a technique for estimating the length and position of a spot event along a weak FBGs cascade sensor. The measurement system is based on the principle of operation of a MWP filter, in particular on the measurement of the electrical S_{21} parameter that characterizes the filter transfer function. A simple configuration is used to interrogate a 5 m-long fiber, containing 500 9 mm-long Bragg gratings, in which the frequency of operation has been swept from 10 MHz to 500 MHz. By evaluating the *FSR'* of the resulting MWP filter, the length of a single hot spot along the very long FBG sensor can be detected with remarkable accuracy under 1 mm. Furthermore, by using a reference tap, the position of the middle point of the spot event can be estimated and referred to the end of the DUT, by using the IFT of the measured RF transfer function (S_{21} parameter). The temperature of the hot spot can be easily evaluated with an accuracy of 1 °C, by controlling the central wavelength of the tunable band-pass filter, without using any more devices or additional wavelength-scanned systems. The sensor temperature resolution is actually limited by the transition slope of the optical band-pass filter. However, the purpose of this contribution was to present and demonstrate the feasibility of this FBGs cascade device as a temperature/strain sensor, by using a photonics-assisted technique. The temperature resolution certainly may be improved by using a tunable optical filter with a high abrupt transition slope.

We have investigated the capability of the proposed system to detect the length and location of spot events, demonstrating a minimum detectable length under 26.5 cm. Actually, this value arises from the modest bandwidth of only 500 MHz used to perform the experiment. Even so, it is possible to release this limitation if the number of replicas of the MWP filter is increased, either by extending the frequency range or by mathematically improving the algorithm used for calculating the IFT. The latter point is actually a complementary research under study going beyond the scope of this paper.

The spatial accuracy under 1 mm has been demonstrated, which is dictated by the instrumental spatial resolution. Hence, since the spatial accuracy basically depends on the system frequency step, the proposed scheme is able to reach the same performance in terms of accuracy even if the length of the sensing device is enhanced. This statement has been validated by performing a set of numerical simulations assuming an array of FBGs having lengths of two or three orders of magnitude longer than the proposed DUT.

Finally, it is worth mentioning that the proposed configuration can also be used to implement a crack/strain sensor. Besides, the use of a BBS relieves the complexity and the cost for stabilization control on light source, and since MW frequencies changes were measured, the influence of the intensity noise of the incoherent source does not lead to resolution impoverishment. Furthermore, although the use of a VNA may enhance the system complexity and expense, the instrumentation required could be simplified by replacing the VNA with an oscillator and a device able to analyze the magnitude response of the MWP filter generated. The simple proposed scheme proves to be cost effective and intrinsically robust against environmental changes and easy to reconfigure.

References

[1] J. López-Higuera, *Handbook of Optical Fibre Sensing Technology*. Hoboken, NJ, USA: Wiley, 2002. [Online]. Available: http://books.google.es/books?id=MglgfUoBMpMC
[2] A. Kersey *et al.*, "Fiber grating sensors," *J. Lightw. Technol.*, vol. 15, no. 8, pp. 1442–1463, Aug. 1997.
[3] S. Y. Li, N. Q. Ngo, S. C. Tjin, P. Shum, and J. Zhang, "Thermally tunable narrow-bandpass filter based on a linearly chirped fiber Bragg grating," *Opt. Lett.*, vol. 29, no. 1, pp. 29–31, Jan. 2004. [Online]. Available: http://ol.osa.org/abstract.cfm?URI=ol-29-1-29
[4] H. Uno, A. Kojima, A. Shibano, and O. Mikami, "Optical wavelength switch using strain-controlled fiber Bragg gratings," in *Proc. SPIE*, 1999, pp. 274–277. [Online]. Available: http://dx.doi.org/10.1117/12.347816
[5] J. Azaña and M. Muriel, "Temporal self-imaging effects: Theory and application for multiplying pulse repetition rates," *IEEE J. Sel. Topics Quantum Electron.*, vol. 7, no. 4, pp. 728–744, Jul. 2001.

[6] M. Volanthen, H. Geiger, and J. Dakin, "Distributed grating sensors using low-coherence reflectometry," *J. Lightw. Technol.*, vol. 15, no. 11, pp. 2076–2082, Nov. 1997.

[7] H. Murayama *et al.*, "Distributed strain measurement with high spatial resolution using fiber Bragg gratings and optical frequency domain reflectometry," presented at the Optical Fiber Sensors Conf., Cancun, Mexico, 2006, Paper ThE40. [Online]. Available: http://www.opticsinfobase.org/abstract.cfm?URI=OFS-2006-ThE40

[8] K. Hotate and K. Kajiwara, "Proposal and experimental verification of Bragg wavelength distribution measurement within a long-length FBG by synthesis of optical coherence function," *Opt. Exp.*, vol. 16, no. 11, pp. 7881–7887, May 2008. [Online]. Available: http://www.opticsexpress.org/abstract.cfm?URI=oe-16-11-7881

[9] J. Sancho, S. Chin, D. Barrera, S. Sales, and L. Thévenaz, "Time-frequency analysis of long fiber Bragg gratings with low reflectivity," *Opt. Exp.*, vol. 21, no. 6, pp. 7171–7179, Mar. 2013. [Online]. Available: http://www.opticsexpress.org/abstract.cfm?URI=oe-21-6-7171

[10] A. L. Ricchiuti, D. Barrera, S. Sales, L. Thévenaz, and J. Capmany, "Long fiber Bragg grating sensor interrogation using discrete-time microwave photonic filtering techniques," *Opt. Exp.*, vol. 21, no. 23, pp. 28 175–28 181, Nov. 2013. [Online]. Available: http://www.opticsexpress.org/abstract.cfm?URI=oe-21-23-28175

[11] L. Thévenaz, S. Chin, J. Sancho, and S. Sales, "Novel technique for distributed fibre sensing based on Faint Long Gratings (FLOGS)," in *Proc. SPIE*, 2014, pp. 91576W-1–91576W-4. [Online]. Available: http://dx.doi.org/10.1117/12.2059668

[12] M. Li, W. Li, J. Yao, and J. Azana, "Femtometer-resolution wavelength interrogation of a phase-shifted fiber Bragg grating sensor using an optoelectronic oscillator," presented at the Advanced Photonics Congress, Colorado Springs, CO, USA, 2012, Paper BTu2E.3. [Online]. Available: http://www.opticsinfobase.org/abstract.cfm?URI=BGPP-2012-BTu2E.3

[13] X. Zou *et al.*, "Optical length change measurement via RF frequency shift analysis of incoherent light source based optoelectronic oscillator," *Opt. Exp.*, vol. 22, no. 9, pp. 11 29–11 139, May 2014. [Online]. Available: http://www.opticsexpress.org/abstract.cfm?URI=oe-22-9-11129

[14] Y. Deng, M. Li, N. Huang, H. Wang, and N. Zhu, "Optical length-change measurement based on an incoherent single-bandpass microwave photonic filter with high resolution," *Photon. Res.*, vol. 2, no. 4, pp. B35–B39, Aug. 2014. [Online]. Available: http://www.opticsinfobase.org/prj/abstract.cfm?URI=prj-2-4-B35

[15] J. Capmany, B. Ortega, D. Pastor, and S. Sales, "Discrete-time optical processing of microwave signals," *J. Lightw. Technol.*, vol. 23, no. 2, pp. 702–723, Feb. 2005.

[16] J. Capmany *et al.*, "Microwave photonic signal processing," *J. Lightw. Technol.*, vol. 31, no. 4, pp. 571–586, Feb. 2013.

[17] *Fbgs-Draw Tower Gratings*. [Online]. Available: http://www.fbgs.com/home/

[18] B. Saleh and M. Teich, *Fundamentals of Photonics*, Wiley Series in Pure and Applied Optics. Hoboken, NJ, USA: Wiley, 2007. [Online]. Available: http://books.google.es/books?id=Ve8eAQAAIAAJ